RT SOLUTIONS, Inc.
9 Channing Street, Cambridge, MA 02138.

Final Report
O3MSAF-VS, 31 December 2008

Improvements in GOME-2 Total Column Retrievals with Clouds as Scattering Layers: Alternative to the CRB Approach

PART 1

Robert J. D. Spurr[(1)]

Walter Zimmer[(2)], Diego Loyola[(2)]

[(1)]*Director, RT Solutions, Inc.*
9 Channing Street, Cambridge, MA 02138

[(2)] *German Aerospace Center (DLR)*
Remote Sensing Technology Institute (IMF)
PO Box 1116, D-82234 Wessling, Germany

31 December 2008

Contractual Manager

Seppo Hassinen
Finnish Meteorological Institute,
P.O.BOX 503, FIN-00101 Helsinki, Finland

RT Solutions, Inc.
9 Channing Street, Cambridge, MA 02138, USA
Email: rtsolutions@verizon.net

Tel: +1 617 492 1183
Fax: +1 617 354 3415
EIN: 20 1995227

1. Introduction

1.1 Current cloud algorithms

For GOME and GOME-2 operational processing, cloud information is obtained using two separate processes. One is an optical recognition algorithm (OCRA) based on threshold techniques using the ancillary polarization measurements made by these instruments. The OCRA algorithm uses a cloud-free composite against which all subsequent reflectances are compared. For details on the GOME application, see [*Van Roozendael et al*., 2006]. OCRA delivers cloud fraction only; it has been validated against synoptic observations [*Tuinder et al.*, 2004] and MSG data [*Loyola et al*., 2007], and it was compared to FRESCO and ICFA results The current GOME-2 OCRA implementation will be used "as is" in the present work.

The cloud fractional cover from OCRA is a fixed input to the ROCINN algorithm [*Loyola*, 2004]. This is a neural network inversion model based on a training set of GOME or GOME-2 Channel 4 O_2 *A* band reflectances in the range 758 to 771 nm [*Loyola*, 2004; *Van Roozendael et al*., 2006]. The forward model is based on the Independent Pixel Approximation (IPA), in which the total reflectance is a linear weighted sum of clear-sky and cloudy reflectance values (c_f is the cloud fraction):

$$R_{sim}(\lambda) = c_f \left\langle R_c(\lambda, \Theta, c_a, c_z) \right\rangle + (1 - c_f) \left\langle R_s(\lambda, \Theta, s_a, s_z) \right\rangle \qquad (1)$$

Here, $\langle R \rangle$ denotes the convoluted reflectance to cloud-top or surface for path geometry Θ (solar zenith angle and line-of-sight angle), wavelength λ, surface albedo s_a and cloud-top albedo c_a, and lower boundary heights s_z (surface) and c_z (cloud-top). The cloudy-sky computation is based on the treatment of cloud as a Lambertian reflecting boundary, but now the cloud-top albedo c_a is to be determined from the inverse model, along with the cloud-top height c_z. Quantities s_z and s_a are from a suitable database and assumed known. Reflectivities must first be calculated on a high-resolution wave number grid using line spectroscopic information for the O_2 *A* band, and then convolved with the instrument response function. For GOME-2, there are 62 wavelengths in the 758-771 nm range.

Simulated reflectances for the GOME-2 ROCINN algorithm have been created using the LIDORT and VLIDORT multiple scattering radiative transfer models. ROCINN has been validated against MSG data [*Loyola et al.*, 2007] and compared to FRESCO, ICFA and SACURA results.

Cloud information (cloud-top albedo and height from ROCINN, cloud fraction from OCRA) is used verbatim in the GOME-1/GOME-2 DOAS algorithms for total column retrieval of O_3 and NO_2. This approach is known as the "clouds as reflecting boundaries" (CRB) model; it is also called the Lambertian Equivalent Reflectivity or LER model.

1.2 Limitations of the CRB model

The CRB approach is not an accurate representation of atmospheric scattering in the presence of clouds, as it fails to account for any transmission of radiation in and through cloud layers [*Ahmad et al*., 2004]. The accuracy of retrieved tropospheric NO_2 and ozone can be seriously

compromised with the CRB assumption. Uncertainties on assumed cloud-model parameters are among the most important error sources in the retrieval of the tropospheric NO_2 column. For polluted scenarios, [*Boersma et al*., 2004] found errors of up to 30% in the tropospheric NO_2 column due to cloud parameter uncertainty. For tropospheric ozone, retrieval schemes using the CRB approach overestimate the column ozone [*Ahmad et al*., 2004]. Moreover, errors on the ozone total column retrieval can be significant when the intra-cloud ozone is not considered - this effect is typically 5-13 DU on average over the Atlantic and Africa [*Liu et al*., 2004].

In the total column algorithms, the intra-cloud ozone column is improperly modeled in the CRB/LER approach. In DOAS algorithms, the mixed-scene air mass factor (AMF) is a weighted mean of individual AMFs to ground and to cloud-top, and the ozone column below cloud-top is the ghost column. The latter is taken from climatology; in reality, intra-cloud ozone may have a significant effect on the backscatter signal [*Liu et al*., 2004]. Recently, Loyola has developed a simple correction for the LER algorithms [*Loyola*, 2007b]. The total column below cloud-top is actually the sum of the "intra-cloud" ozone column (V_{ic}) plus the column below the cloud itself. In reality, backscatter measurements are sensitive to V_{ic}, and the traditional LER methods will overestimate the total atmospheric column by ignoring V_{ic}. The study by [*Liu et al*., 2004] showed that total column errors could be large when V_{ic} is not accounted for. The Semi-transparent Lambertian cloud (STLC) model [*Loyola*, 2007b] provides an initial empirical characterization of V_{ic} as function of the climatological ozone column below cloud-top, the cloud albedo, and the solar zenith angle. An analysis of 6 months of recent GOME-2 results shows that the overestimation is reduced on average from 3.37% for the traditional LER method to 1.64% for the SLTC mode.

1.3 Objectives and scope of document

In this work, we present a different approach to the retrieval of cloud information from the ROCINN algorithm, and the usage of this information in total column trace gas retrievals in the UV and visible GOME-2 spectral channels. The basic assumption of a cloud as reflecting boundary (CRB) will be contrasted with the more realistic treatment of cloud layers as optically uniform media of water droplet scattering particles with optical properties described by Mie theory. We call this the clouds-as-layers (CAL) treatment. In this regard, the cloud-top height, the cloud geometrical thickness and the cloud optical thickness are the defining *macroscopic* characteristics. With CAL, it is necessary to employ full multiple scattering radiative transfer (RT) modeling for the whole atmosphere, including cloud layers; the idea of a retrievable cloud-top albedo is abandoned (cloud BRDFs and albedos can be computed directly from the RT model as diagnostics).

The major objective of this work is to show that operational total column retrievals in UPAS can be improved with the use of the CAL scheme in the forward model interfaces in both the trace gas UV/visible retrievals and in the ROCINN algorithm. In order to achieve this objective, we delineate three stages to this work:

1. Development of a new set of reflectance templates for ROCINN in order that the algorithm can now deliver the necessary CAL information;
2. Development and testing of forward model interfaces for computing AMFs using the

CAL model;

3. Delivery of new total column results based on the CAL treatment, and initial analysis of the results for a limited set of validation orbits.

This work was funded through an O3MSAF 2008 Visiting Scientist Grant awarded to RT Solutions Inc., for the period 1 January 2008 through 30 September 2008 with an extension to 31 December 2008. This is the final report for this work.

Work done on the implementation of the first two objectives was summarized in the Interim Report of 30 June 2008 covering the first 6 months of the grant period. This material is given again in the present document, though in slightly modified form. Neural network training for the new CAL-based ROCINN reflectance templates has not been completed in time for the end of the study period, and so an alternative derivation of cloud-layer optical thickness was used instead [*Loyola et al*., 2009]. The new work reported here concerns the third objective in the above list. The scope of the report is as follows.

In section 2, the CRB and CAL layering schemes are summarized, and the optical property setup for these schemes is described. In section 3, we report on sensitivity of satellite radiances to the cloud-layering scheme in general and to the assumed microphysical parameters that specify cloud particle scattering. In section 4, we look at CAL schemes for the ROCINN cloud property algorithm – this includes the newly classified reflectance template database based on CAL, and the use of an alternative scheme to generate cloud optical thickness from ROCINN-retrieved albedos. In section 5, we summarize LIDORT settings and performance aspects for the UPAS implementations.

In section 6, we look at complete total O_3 and total NO_2 results for one GOME-2 orbit. All retrievals were done using the DOAS method. We look at clear sky AMFs ("to the ground") and AMFs in the presence of clouds (CRB and CAL), along with their dependencies on cloud-top height and other parameters, and differences in the final VCD values. For the revised CRB scheme, results are close to current operational values. We present results using the CAL scheme, and note some of the contrasts with the CRB results and the differences. In section 7, we look forward to the validation phase for the new layering scheme.

2. Cloud layering schemes and IOP preparation

2.1 Current CRB scheme in UPAS

Figure 1 is a sketch of the current atmospheric layering scheme for calculating simulated reflectances (this applies equally to DOAS-type UV/visible trace gas retrievals and to the ROCINN templates). In the clear sky case (left panel), the layer containing the cloud-top level is not subdivided. In the cloudy case (right panel), a reduced layer is used immediately above cloud-top, with temperature, pressure and trace gas content in the original layer adjusted to the cloud-top height via linear or log-linear interpolation. Because of this adjustment, optical properties in this layer are not consistent between the clear-sky and cloudy case. The only other piece of information needed to specify the cloud is its albedo.

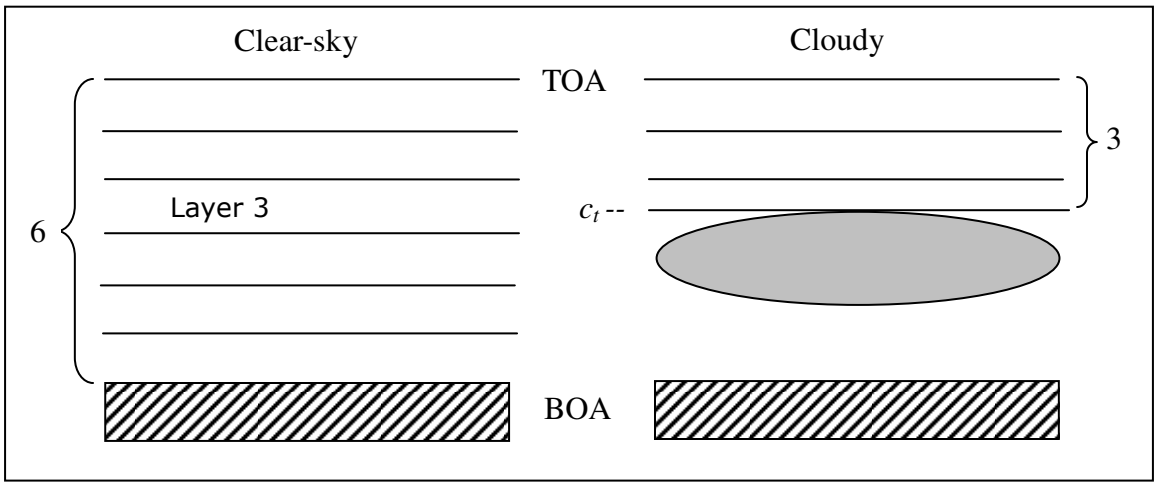

Figure 1. Current CRB scheme in GOME-2 forward models. In the sketch, there are 6 clear-sky layers and 3 layers for the cloudy atmosphere. Layer 3 is not the same in the cloudy situation.

2.2 New CAL and CRB layering schemes

Figure 2 shows the CAL case, with two boundaries for cloud-top c_t and cloud-bottom c_b. We subdivide the height-grid layers, again using linear or log linear interpolation to define temperatures and pressures at boundaries, and adjusted trace gas amounts in the reduced layers. If the cloud is entirely contained in one original layer, this layer will be given two subdivisions. In general, we increase the number of layers by 2 in the presence of a layer cloud. If one of the cloud boundaries coincides with one of the original height grid levels, then only one subdivision and additional layer is required. This scheme will also work with cloud at the ground (fog).

In contrast with the CRB case, all atmospheric layers are included in simulations with clouds. Indeed, for consistency, we use the same layering for the clear sky simulations as used for atmospheres with the cloud layer. This ensures that properties of the atmosphere below and above the cloud layers are the same in both cases. It also ensures that within the cloud, atmospheric properties (apart from the cloud itself) are also the same. The cloud is regarded as

optically uniform of total optical thickness τ_c; thus, optical thickness values for each layer n within the cloud are parceled out according to the geometrical thickness of the layer as a ratio of the total geometrical thickness $c_g = c_t - c_b$ of the cloud. Note that τ_c must be specified at one wavelength (we take the value at 758 nm) – once τ_c is known, the total particle loading is set, and optical thicknesses at other wavelengths is determined from Mie calculations at these wavelengths. Cloud water droplets exhibit almost conservative scattering, with the optical thickness at 325 nm varying only slightly from its value at 758 nm.

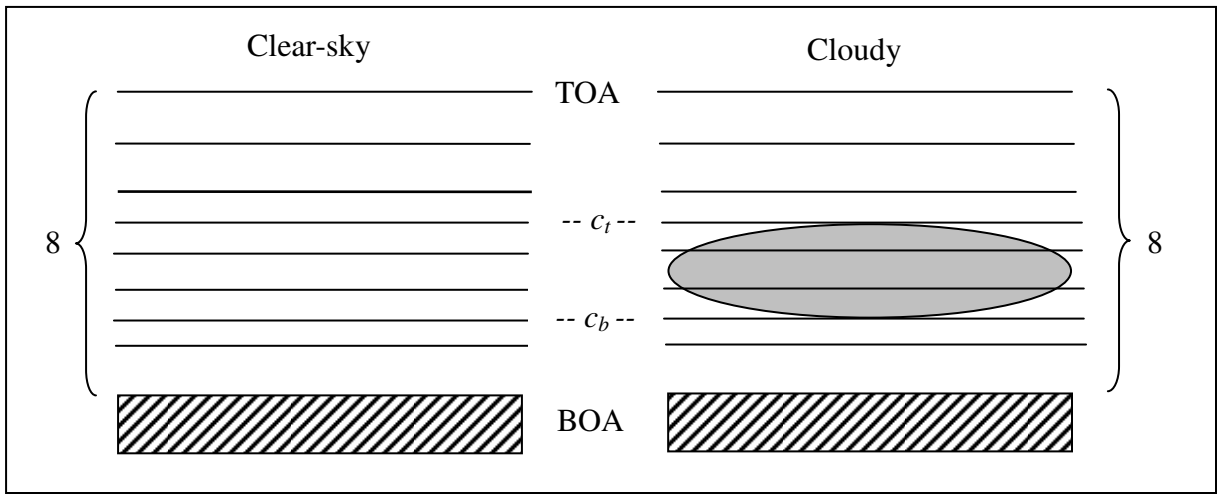

Figure 2. CAL scheme in GOME-2 forward models. Boundaries for cloud-top c_t and cloud-bottom c_b define two additional layers that are used in both situations.

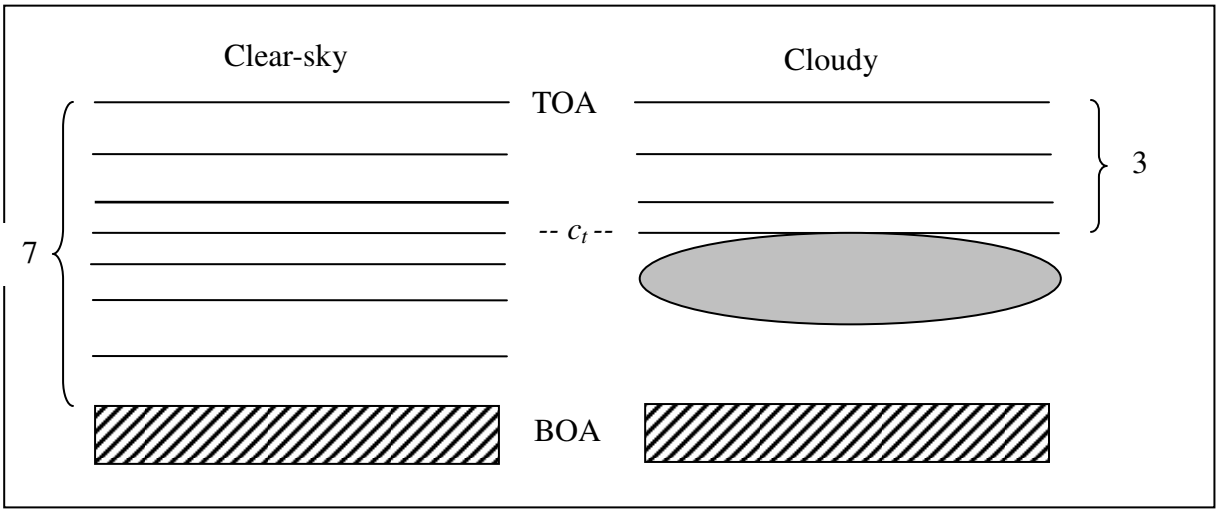

Figure 3. Revised CRB scheme in GOME-2 forward models. Boundary for cloud-top c_t defines one additional layer for the clear sky case.

In addition to the cloud layer boundaries (which specify the geometrical thickness), we require the cloud optical thickness and a specification of the microphysical cloud properties. The former is a retrieval parameter to be extracted from a new CAL-based ROCINN algorithm; the latter are

assumed known from Mie theory. However, the CAL scheme is not wholly consistent with the CRB layering as described in Figure 1, so we have adopted a *revised* CRB gridding scheme (Figure 3), which always uses the reduced layer immediately above cloud-top, thus ensuring that clear-sky and cloudy simulations are based on the same atmosphere above cloud-top. This revised CRB scheme introduces a single extra layer in the clear sky simulations. It is anticipated that there will be small differences in TOA radiances calculated using the two CRB schemes.

2.3. Optical property setups for CAL

We require the total overall optical properties $\{\Delta_n, \omega_n, \beta_{ln}\}$ in each layer n. These are the layer extinction optical depth, the total layer single scattering albedo and the total layer phase function expansion coefficients (scalar RT with no polarization). For a clear sky layer, the first two are given by (we assume Rayleigh scattering and single-species absorption):

$$\Delta_n = U_n \alpha_n + A_n \sigma_{Ray} \quad ; \qquad \omega_n = \frac{A_n \sigma_{Ray}}{\Delta_n} \tag{2}$$

Here the layer trace gas amount is U_n, with trace absorption cross section α_n; A_n is the air density for Rayleigh cross-section σ_{Ray}. For Rayleigh scattering $\beta_0 = 1$, with $\beta_2 = (1-\rho)/(2+\rho)$ in terms of depolarization ratio ρ. Values of ρ and σ_{Ray} are taken from [*Bodhaine et al*., 1999].

In the presence of a cloud, for which the optical thickness is τ_n in layer n, we have:

$$\Delta_n = \tau_n + U_n \alpha_n + A_n \sigma_{Ray} \quad ; \qquad \omega_n = \frac{\eta \tau_n + A_n \sigma_{Ray}}{\Delta_n} \tag{3}$$

Here, η is the cloud particle single scattering albedo. The total phase function expansion coefficients are a weighted mean of the Rayleigh and cloud coefficients.

Linearized optical properties are required for a direct fitting retrieval in which the forward model delivers Jacobians with respect to the total column C of ozone, as well as reflectances. Assuming a column-classified ozone climatology that delivers the layer Umkehr amounts U_n as a function of C, then the required linearized inputs may be found by partial differentiation:

$$\frac{\partial \Delta_n}{\partial C} = \frac{\partial U_n}{\partial C} \alpha_n \quad ; \qquad \frac{\partial \omega_n}{\partial C} = -\frac{\omega_n}{\Delta_n} \frac{\partial U_n}{\partial C} \alpha_n \tag{4}$$

The column-profile association assigns a unique profile $\{U_n\}$ as a function of C. For the TOMS Version 8 climatology currently used in GOME-2 total ozone, this association is linear.

For the cloud microphysical quantities, we assume only water-droplet clouds, with refractive index (m_r, m_i), with m_r = 1.34 and $m_i = 10^{-7}$. We take a lognormal particle size distribution having effective radius r_g set to 5.5 microns and standard deviation s_g equal to 0.35. In section 4, we examine sensitivity to these parameters. The single scatter albedo η_c and phase function expansion coefficients emerge directly from Mie calculations. In fact, $\eta_c \approx 1$ at our wavelengths. Phase functions have sharp forward peaks, requiring many expansion coefficients to ensure accuracy with the RT computations (see section 5). We use the linearized Mie model developed by R. Spurr based on the Meerhoff code [*de Rooij and van der Stap*, 1984].

3. Sensitivity studies for CAL in the UV

In all simulations in the UV, the surface is regarded as Lambertian. It is noteworthy that in the CAL scheme, some sensitivity to the surface is present even for a fully cloudy pixel, provided the optical thickness of the cloud is not too large. This is in contrast to the CRB case, where the atmosphere below cloud top is assumed unknown.

In Figure 4, we present some typical results for ozone Air Mass Factors calculated at 325.5 nm. Shown are three AMFs calculated using the CRB scheme and plotted as a function of cloud-top albedo, and three AMFs calculated using the CAL scheme and plotted as a function of cloud optical depth. The total intensity-weighted AMFS are shown here. The three curves correspond to cloud fractions 0.2, 0.5, and 0.8. In both CRB and CAL cases, the cloud top is the same and other atmospheric distributions are the same. Although no direct comparison is possible, it is clear that AMFs using CRB are smaller for all conditions than those found using CAL. In the DOAS algorithm, where the AMF acts as a conversion on the fitted slant column, this observation confirms the tendency to overestimate the vertical column density using CRB. Note the nonlinear shape of the CAL AMFs for cloud optical depth below 30 (cloud-top albedo of ~0.7) in contrast to the almost linear behavior of the CRB AMFs in this region. The vast majority of clouds have an optical depth smaller than 30; on global average the cloud optical depth is 14 for GOME and 9 for ISCCP [*Loyola et al*., 2009].

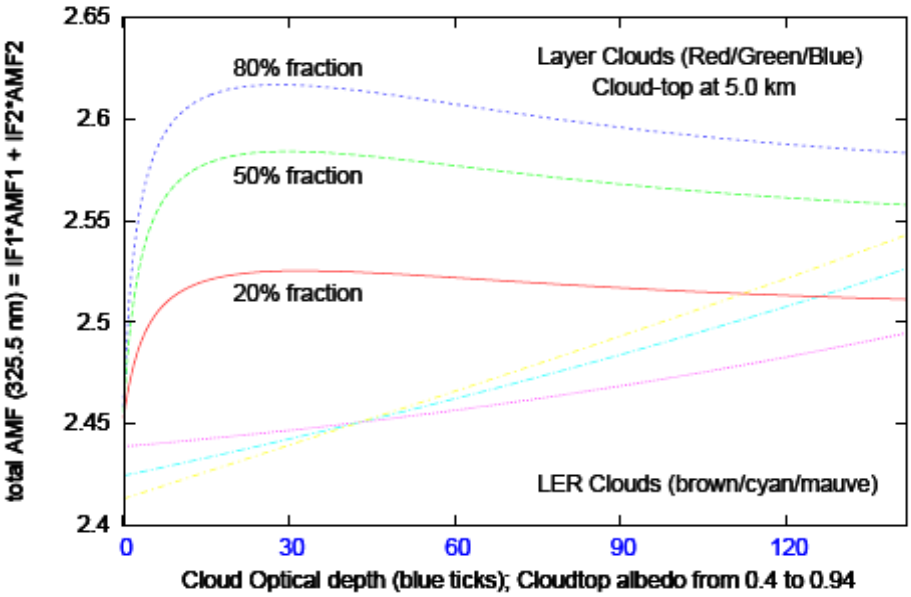

Figure 4. AMFs computed using the CAL scheme (red, green and blue lines), as opposed to the CRB scheme (brown, cyan and mauve lines). Cloud top is at 5.0 km; 3 fractions as indicated.

Cloud-top height and cloud optical thickness values are retrieved from the ROCINN algorithm. However, other parameter values characterizing the layer clouds are sources of "model parameter" error in all algorithms, and it is desirable to know what effect these uncertainties may have on total ozone accuracy, for example. These parameters include the cloud bottom height (or geometrical thickness and the Mie particle size distribution lognormal effective radius and

standard deviation. We are not yet ready to gauge these model parameter effects on total column retrieval accuracy, but we can get a good idea by examining the sensitivity of simulated radiances and total column weighting functions to these parameters. It is desirable that these sources of error should be small.

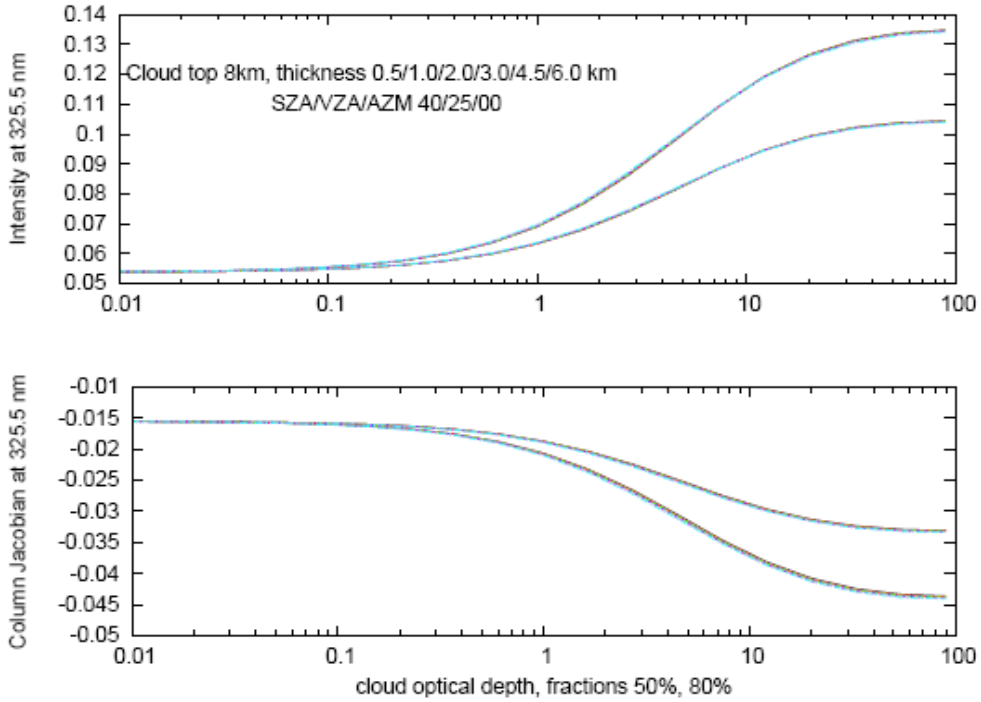

Figure 5. Sensitivity to cloud bottom height. Example for 2 cloud fractions and cloud-top at 6 km.

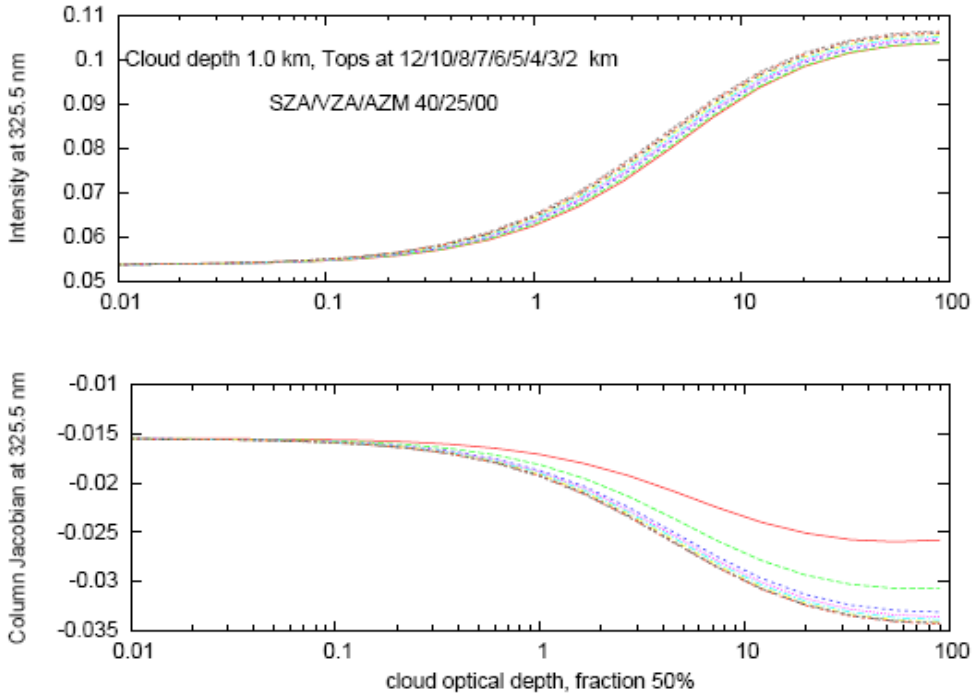

Figure 6. Sensitivity to cloud top height. Example for 2 cloud fractions and cloud thickness of 1 km.

Figure 5 shows the effect of varying the cloud bottom height on TOA radiances (top panel) and total ozone Jacobians (lower panel), assuming a cloud-top at 6 km. Results are shown for one geometry (SZA 40, VZA 25, AZM 0.0) at 325.5 nm, Two sets of curves are shown, corresponding to two choices of cloud fraction (50% and 80%). Six values of the lower boundary height were used (0.5, 1.0, 2.0, 3.0, 4.0 and 5.0 km), and the basic dependence is on cloud optical depth. These results show that the cloud geometrical thickness has little effect on TOA simulations, and this encouraging observation was used to justify the choice of a single bottom height for the cloud reflectance templates in the A-band ROCINN algorithm (see section 5).

It is interesting to turn Figure 5 around and look at the cloud-top sensitivity for one setting of the cloud geometrical thickness. This is shown in Figure 6, where the TOA radiances and total ozone Jacobians have been computed for the same atmosphere and viewing conditions as for Figure 5, but now the cloud-top is allowed to vary from 2.0to 12.0 km as shown, keeping the geometrical thickness constant at 1.0 km. The radiances show surprisingly little sensitivity at all optical depths, but the total column Jacobian shows increasing sensitivity to cloud top height for higher values of the cloud optical thickness.

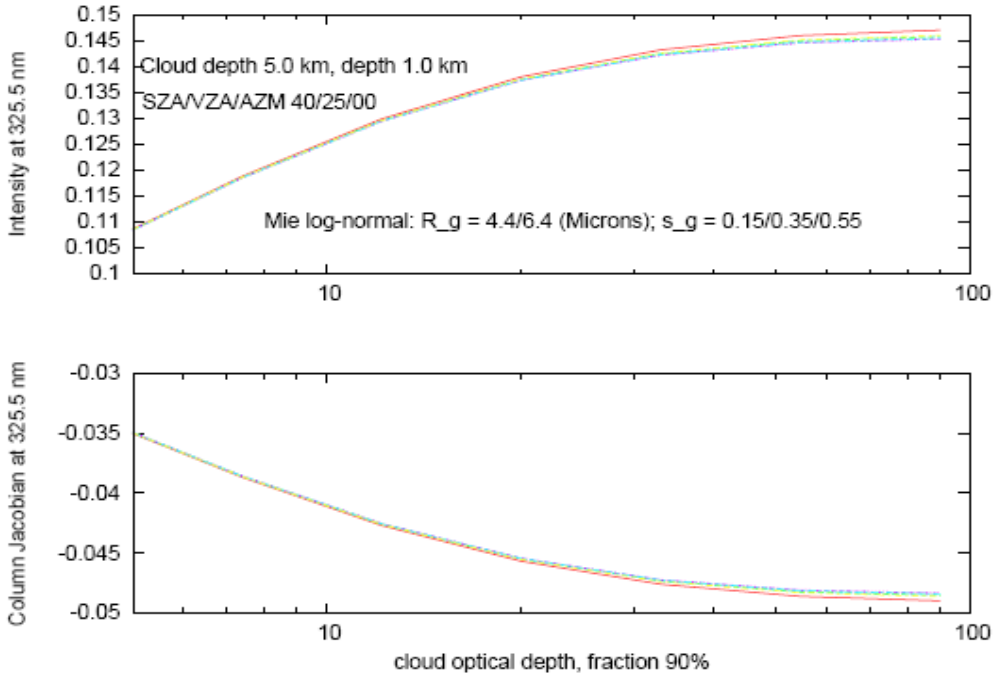

Figure 7. Sensitivity to Mie scattering microphysical parameters. Example for cloud fraction 90% and cloud thickness of 1 km, cloud-top at 5.0 km; geometry and atmosphere as for Figure 5 and 6.

Lastly, in Figure 7, we examine sensitivity with respect to the particle size distribution parameters. For Mie scattering with lognormal size distributions, it is known that the effective radius varies from 4 to 10 microns (μ), with standard deviations in the range 0.2-0.6 μ. Shown in Figure 7 are TOA radiances and total ozone Jacobians plotted against cloud optical depth, for two values of the lognormal effective radius (4.4 and 6.4 μ) and 3 values of the standard deviation (0.15, 0.35 and 0.55 μ). Cloud top was set at 5.0 km with geometrical thickness 1.0 km and fraction 90%; other atmospheric conditions and geometry as in the previous two Figures. The relatively small offsets on these TOA simulations justify the choice of a fixed effective radius and standard deviation.

4. CAL in the ROCINN algorithm

4.1. New CAL-based reflectance templates for ROCINN

Clear sky simulations are characterized by the surface height h_s and surface albedo a_s. In ROCINN, we have taken 6 heights {0.0, 0.5, 1.0, 2.0, 3.0, and 4.0} in [km], and 5 surface albedos {0.02, 0.1, 0.3, 0.6, and 0.98}. For a complete specification of reflectances in the presence of clouds, we must extend the classification used in the older ROCINN algorithms based on the original CRB scheme.

Cloud-top albedo is absent; in addition to cloud-top height c_t, we have the cloud-bottom height c_b (or equivalently the cloud geometrical thickness c_g), and the cloud optical thickness τ_c to characterize the cloud. Ranges for c_t are {0.5, 1.0, 2.0, 3.0, 4.0 and up to 14.0} in [km] (15 values), for c_g {0.2, 0.5, 1.0, 2.0, 4.0, and 8.0} in [km] (6 values), and for τ_c {0.5, 1.0, 2.0, 3.5, 6.0, 10.0, 17.0, 30.0, 50.0, 100.0, and 378.7} (11 values). The last figure here is taken to be the extreme value used in the ISCCP classification [*Hahn et al.*, 2004].

Since the whole atmosphere is used in CAL simulation, we also have the clear sky classifications for surface height h_s and albedo a_s. This 5-dimensional classification for cloud reflectances is too unwieldy, and based on the poor sensitivity to cloud geometrical thickness and surface height in the UV, we have assumed a single surface height of 0.0 km, and a single cloud geometrical thickness as follows. If $c_t = 0.5$, then $c_g = 0.3$; if $c_t = 1.0$, then $c_g = 0.5$; for $c_t = 2.0$. we take $c_g = 1.0$; and for all other c_t values, $c_g = 2.0$ (distances in [km]). We assume the cloud particle distribution function to be log normal with $r_g = 6.0$ and $s_g = 0.3$. Mie output is pre-calculated at two wavelengths and cloud optical properties at other wavelengths are computed by linear interpolation. [For sensitivity studies and other situations, the template environment has the ability to calculate Mie output from scratch]. Simulations have included background aerosols used in the OCO Level 2 retrieval algorithm [*Natraj et al.*, 2008].

For the A-band templates, we calculate at a fine spectral resolution of 0.025 wave number – this amounts to more than 10,500 calculations covering the template range (758-771 nm), before convolution to the GOME-2 resolution (62 points). Line spectroscopic data come from the HITRAN 2004 database [*Rothman et al.*, 2005], with line-by-line cross-section computations using the Voigt line shape; the procedure is the same as before [*Spurr and Loyola*, 2007].

For the LIDORT settings, we use a baseline height grid of 23 layers, with the TOA (top of atmosphere) set at 60 km, and a 1 km resolution up to 10 km, then a 2 km resolution from there to 24 km, then a 3-5 km resolution above this level. This basic layer grid is necessary to minimize discretization errors due to vertical layering. We use 8 discrete ordinates for multiple scatter integration in the polar direction half space. All LIDORT calculations were performed using the "outgoing sphericity correction", in which single scattering is computed to a high level of accuracy for all solar and line-of-sight paths in a curved atmosphere using the new parameterization developed by R. Spurr [*Spurr*, 2008] and installed in VLIDORT and LIDORT in 2007. The delta-M scaling is applied to all cloudy sky computations.

As before, we use 10 solar angles ranging from 15 to 88° and output at 11 viewing zenith angles and 5 azimuth angles. All viewing geometry angles are given at BOA. For the initial set of

templates, we used VLIDORT in scalar mode (polarization not included), and employed the 3-fold CAL classification as noted above (surface albedo, cloud-top height and cloud optical thickness), for a single cloud geometrical thickness and one surface height.

4.2. CAL-based cloud optical thickness from ROCINN albedos

Due to lack of time, the neural network inversion with the new CAL ROCINN templates has not yet implemented. Therefore, we have used an alternative approach to deriving the cloud optical thickness necessary for CAL retrieval studies. This approach is based on radiative transfer simulations to establish a connection between cloud-top albedo and cloud optical thickness. GOME cloud optical thicknesses derived by this method are already part of the operational GOME-2 total column products [*Valks and Loyola*, 2008].

A more detailed description of the optical thickness algorithm and an analysis of results for both GOME-2 and GOME/ERS-2 are given in a forthcoming paper [*Loyola et al*., 2009].

5. LIDORT settings for the UV modeling in UPAS

For the UV, we work with an atmosphere having molecular scattering only, but with trace gas absorption, and cloud scattering only in the appropriate layers according to the CAL gridding scheme. In UPAS, RT calculations are done "on-the-fly" as part of operational DOAS retrieval of total ozone for example. Cloud phase functions are strongly peaked in the forward scattering direction, so in theory, one would need a large number of discrete ordinates in the RT model to allow for an expansion in Legendre polynomials. This would make the RT calculations computationally expensive. In the UV Huggins bands, the dominance of Rayleigh scattering and stratospheric ozone absorption helps to mask cloud effects on TOA radiances. Our goal is to use as few discrete ordinates as possible, but to keep radiance accuracy at a 10^{-4} level.

LIDORT performance is aided by a number of speed enhancements. The first is the well-known Delta-M approximation (phase function truncation) for the multiple scatter calculation. Secondly, we employ the outgoing sphericity correction (solar and line-of-sight paths in a curved atmosphere) for exact single scattering; the delta-M scaling approximation still applies to cloud-filled layers, and the Nakajima-Tanaka ansatz then applies to the single scatter correction itself [*Spurr*, 2002]. It is also possible to apply phase function truncation to the single scatter phase function. Thirdly, we have the "solution saving" and "boundary value telescoping" performance options [*Spurr*, 2008]. Here, it is only necessary to solve the RTE in non-cloud layers for Fourier azimuth components $m = 0$, 1 and 2 (solution saving). For Fourier components $m > 2$, the only active scattering layers are those in the cloud, and it is then possible to use a reduced solution of the boundary value problem just for these active layers (the telescoping option).

# Discrete ordinates	Regular delta-M	Exact sing scatter ?	Addl. SS scaling ?	Radiance Value	% diff. to "truth"	Runtime (secs)
50	✓	×	×	0.014300	+0.28	10.74
20	✓	×	×	0.014388	+0.33	0.743
10	✓	×	×	0.014314	-0.18	0.096
50	✓	✓	×	0.014340	----	7.55
20	✓	✓	×	0.014344	+0.03	0.443
10	✓	✓	× (500)	0.014344	+0.03	0.073
4	✓	✓	✓ (50)	0.014283	- 0.40	0.012
4	✓	✓	✓ (110)	0.014376	+0.32	0.012
4	✓	✓	✓ (180)	0.014340	0.00	0.012

Table 1. Initial performance estimates for a cloudy scenario in the UV (see text for details). LIDORT Calculations were done on a Dell 8400 3.8 GHz Dimension computer at RT Solutions.

Table 1 contains some initial performance estimates for a mostly cloudy scenario: the fractional cover was taken to 95%, with a cloud of optical thickness 20.0 between 3 and 10 km situated in a

23-layer atmosphere with Rayleigh scattering and ozone absorption (total column 350 DU) , and surface albedo 0.05. Calculations were done at 325.51 nm, with solar zenith angle 82°, viewing angle 40°, and relative azimuth 0°. 500 expansion coefficients were retained for the cloud phase function. Comparisons were done against a "truth" simulation with 100 discrete ordinates and all options turned on. It turns out that it is necessary at all times to use the multiple scattering delta-M scaling, and to include the exact single scatter computation. The additional scaling on the single scatter computation (column 4 in the table) is useful – we can achieve out 10^{-4} accuracy criterion with only 4 discrete ordinates in the half space, provided we truncate and scale the exact single scatter phase function expansion at moment number 180 (final row).

These LIDORT settings have been established for the UPAS calculations. A Mie database of cloud scattering properties has been added to the UPAS system – the main input here is the list of cloud scattering phase function expansion coefficients (we have allowed for 300 of these in the exact single scatter computation).

Note on performance. For an initial set of 4 orbits (section 6.4), it was found that the UPAS calculation time with CAL treatment is about 15% longer than the time taken using the CBR treatment for the same orbits. This is well within the data turnover rate for DOAS retrieval, since the AMF calculations are only for one wavelength (for a partially cloudy pixel requiring 3 iterations for the vertical column density, there will be 12 calls to LIDORT). This means that CAL approach can be also used for the calculation of the GOME-2 total column products in near real time.

6. Initial whole-orbit results with CRB and CAL schemes

6.1. Results for GOME-2 orbit 2326 for CRB schemes

First, we present some results using clouds as reflecting boundaries (CRB). For GOME-2 orbit 2326 (a North-South orbit over-passing Western Europe on April 1st, 2007), we look at the relative differences between total-O_3 and total-NO_2 AMFs and vertical column densities (VCDs) calculated with the original CRB scheme (see sketch in Figure 1) and calculated with the new scheme (Figure 3 sketch). We would expect differences to be small for ozone, since most of the column is in the stratosphere. This is indeed the case, as is seen in Figures 8 and 9, which show differences in the AMFs to ground and in the VCD. Results are plotted against pixel numbers (top panels) and against ROCINN-retrieved cloud-top height (lower panels). Results are shown separately for forward scans (green, red, and blue) and the back scan (magenta).

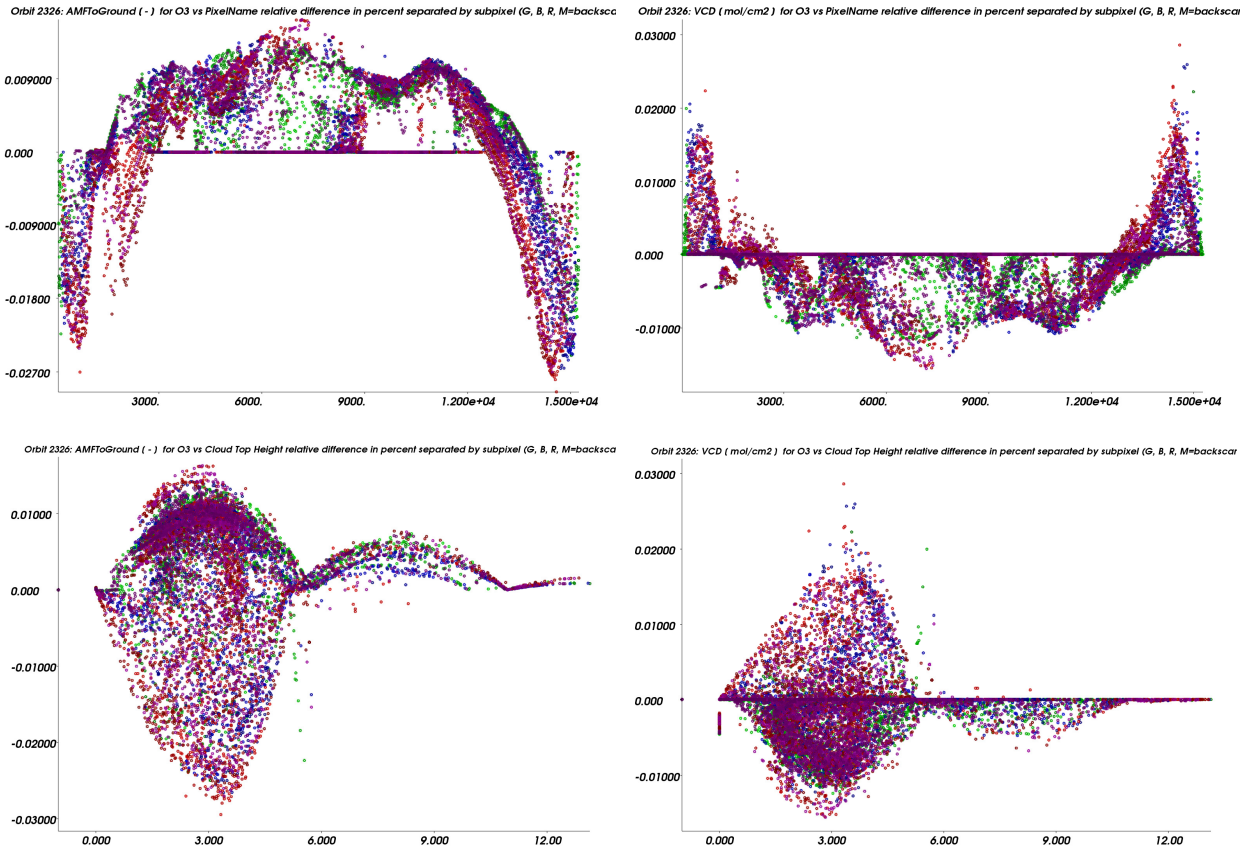

Figure 8. Ground AMFs and VCDs for Total column O_3: Relative differences (in %) due to old and new CRB layering schemes for the GOME-2 orbit # 2326, by pixel number (left panels) and against cloud-top height (right panels).

In all cases, differences are small. There is a very weak solar angle dependency with pixel number across the orbit; this is attributable to the more precise nature of the new CRB layering scheme. This dependency is not a significant source of error.

The lower panels highlight the dependency with retrieved cloud-top height. This is present even in the clear-sky calculation of AMF (bottom left), because the new layering scheme introduces an interim height level which is the cloud-top height into all computations (with the exception of a pixel that has been flagged completely cloud-free). This dependency is also weak. There is also some structure based around the four lowest pressure levels in the TOMS V8 ozone climatology (this grid is the standard layering in the algorithm). These levels are at 1013 mb, 512 mb, 256 and 128 mb corresponding to zero, one, two or three scale heights above the ground (0.0, ~5.6, ~11.2 km and ~16.7 km). The new CRB layering scheme introduces a new level somewhere between these scale heights; interpolation of atmospheric distributions must be done to this level, and the interpolation error is largest at points furthest from these scale height 'nodes'.

Differences for AMFs to cloud-top (not shown here) are in general an order of magnitude smaller than those for AMFs to ground, shown in Figure 9. VCD differences are small (nowhere outside the range -0.015% to 0.03%), indicating that for ozone, the CRB layering scheme is not a significant source of uncertainty.

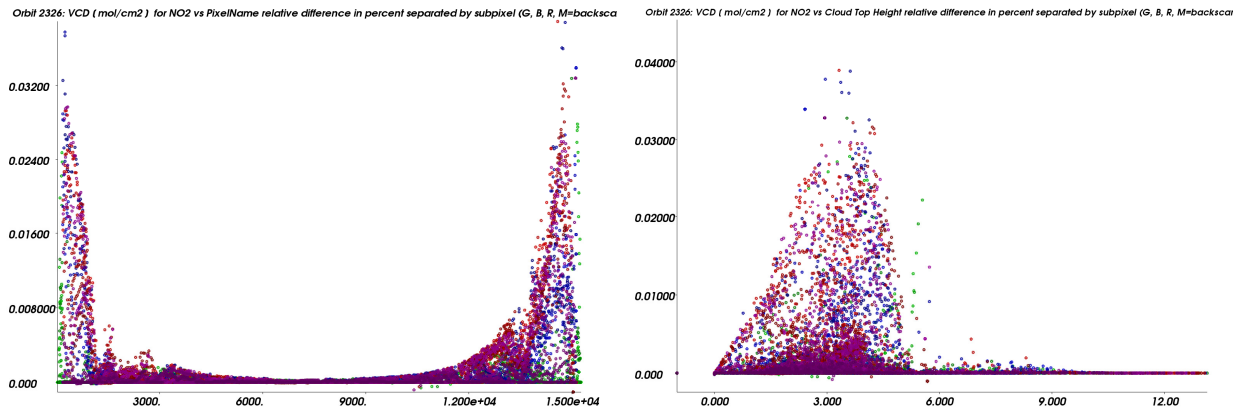

Figure 9. Total column NO_2 VCD differences due to old and new CRB layering schemes for the GOME-2 orbit # 2326, by pixel number (left panel) and against cloud-top height (right panel).

Figure 9 shows corresponding results for NO_2 VCD. The general pattern of results is similar, and once again, the choice of CRB layering scheme seems to have little effect on DOAS accuracy with reflecting clouds. VCD differences are small (nowhere above 0.04%).

6.2. Total O_3 results for GOME-2 orbit 2326: CAL vs. CRB

Here, we present differences in AMFs and VCDs calculated first with the new CAL scheme (Figure 2 sketch), and second with the old CRB scheme which is the current operational default. This comparison is not just a question of level interpolation. CAL calculations depend upon a completely different physical representation of clouds (one that is in principle a great deal more realistic than the CRB Lambertian-albedo scenario). We would therefore expect results to be somewhat different, especially for ozone, for which absorption is larger than optically thin NO_2, and which is more sensitive to stronger light scattering in the UV.

Cloud microphysical scattering properties have been discussed in previous sections. With the CAL scheme, the cloud-top is taken from ROCINN, along with cloud-top albedo. The latter is

then used as a proxy for cloud optical thickness via the NN algorithm noted in section 4.2. Cloud bottom height is taken to be 2 km beneath cloud top for $h_{\text{ctop}} > 2$ km, 1 km for $1 < h_{\text{ctop}} < 2$, and 0.5 for $h_{\text{ctop}} < 1$. (The study in section 4 demonstrated the insensitivity to this parameter).

It should be noted again that there is no ghost column in the CAL scheme – the ozone content of the atmosphere below cloud-top is accounted for explicitly in the layering scheme. The defining equation for VCD is then:

$$V = \frac{E}{(1-\phi)A_{clear}^{CAL} + \phi A_{cloud}^{CAL}} \tag{5}$$

where E is the slant column, ϕ the intensity-weighted cloud fraction, and $A_{clear}^{CAL}, A_{cloud}^{CAL}$ are the AMFs computed with the CAL model for clear sky and for cloudy conditions.

The next set of Figures are similar in scope to Figures 8 and 9, again showing a whole GOME-2 orbit of results for total column ozone and nitrogen dioxide VCDs and their associated AMFs. We also show the *cloud* AMFs in this work (these are AMFs computed in the presence of a scattering cloud layer, ***NOT*** the AMFs "to cloud-top"). The results will also show some additional dependencies.

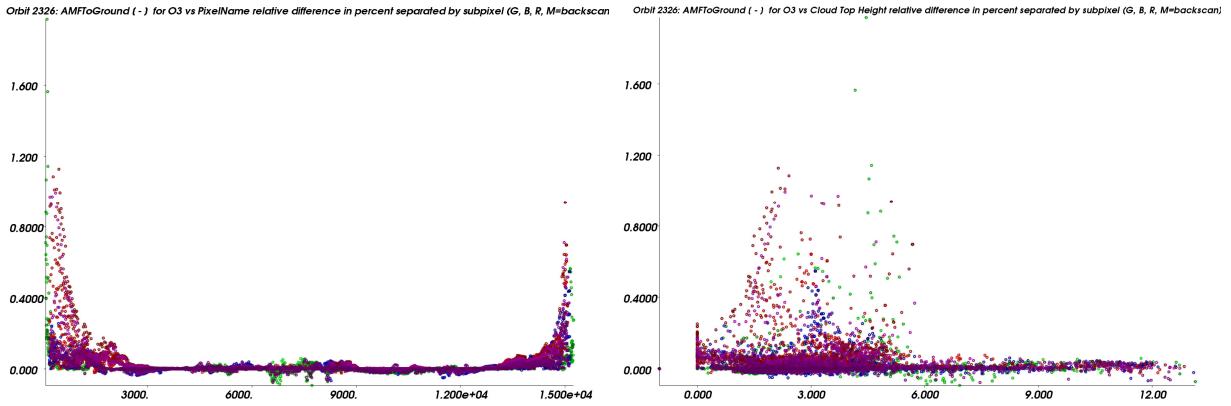

Figure 10. Total column O_3 clear sky AMFs: differences between the CAL and old CRB layering schemes for the GOME-2 orbit # 2326, by pixel number (left panel) and cloud-top height (right panel).

We start with the O_3 AMFs for a clear sky scenario (Figure 10), plotted against pixel position (left panel) and cloud-top height (right panel). It is clear that the CAL values are close to their CRB counterparts for the vast majority of cases. Differences are not quite as low as in the previous section where we compared CRB schemes; this is because the CAL scheme introduces two additional levels in the layering scheme. All the outliers occur at the orbit extremes where the SZA is large (left panel); further, these situations occur only for low clouds below the first TOMS scale height at ~5.6 km (right panel).

Figure 11 shows CAL/CRB differences in O_3 AMFs in the presence of cloud. Here we expect quite different results: on the one hand, the CRB calculation assumes a Lambertian albedo at cloud top, while the CAL calculation includes ozone all the way to ground level, and will depend on scattering in the lowest layers of the atmosphere below cloud-top, and also on the surface reflecting property (not to mention boundary layer aerosols). Actually, it is not altogether

meaningful to make this comparison, since the CAL and CRB AMFs are used differently in the respective VCD calculations.

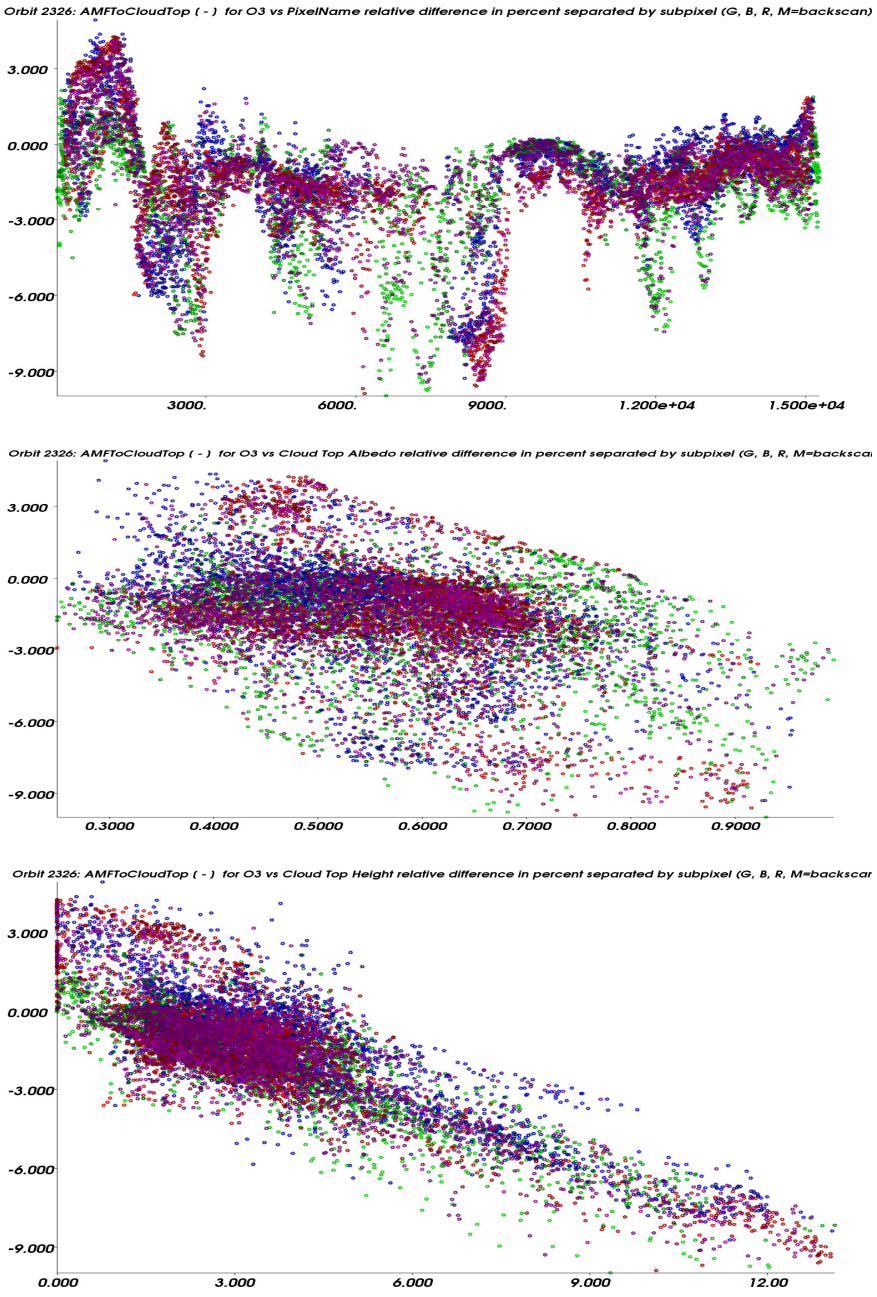

Figure 11. Total column O_3 cloudy sky AMFs: differences between the CAL and old CRB layering schemes for the GOME-2 orbit # 2326, by pixel number (top panel), cloud-top albedo (middle panel) and cloud-top height (bottom panel).

Over the orbit, the AMF differences are now closely linked to the presence of cloud layers (top

panel). There is a barely discernible pixel dependence, which mirrors the SZA dependence. Plotting these results again, this time against cloud-top albedo (middle panel), we see there is a broad negative bias of around 1.5%, but there is little evidence of a gradient in this bias. The lower panel shows the results again, this time against cloud-top height, and here there is a clear gradient with increasing cloud-top height. The latter reflects the increasing presence of ozone in the clouds as we drop further into the troposphere (the CRB calculation has no *atmosphere* beneath cloud-top).

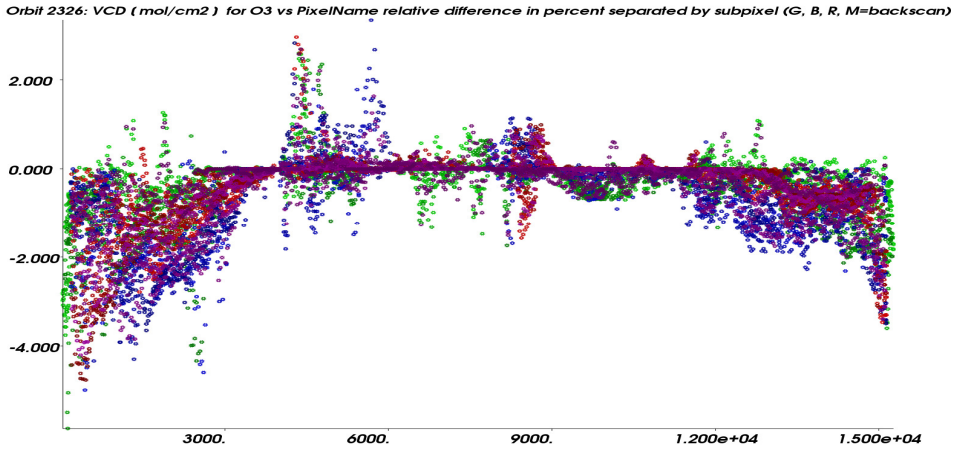

Figure 12. Total column O_3 VCDs: differences between the CAL and old CRB layering schemes for the GOME-2 orbit # 2326, by pixel number.

In Figure 12, we show the orbit of VCD difference results for ozone. Here, the clustering is closer to zero – the strong dependence on cloud presence (Figure 11, top panel) is compensated by the lack of a ghost column and V_{ic} correction term in the VCD calculation with CAL-derived AMFs. The presence of clouds can lead to results that differ by as much as ±2% for pixels 4000-12000. More evident is the SZA drift at the orbit extremes, where there is a clear negative bias below pixel 4000 and above pixel 12000. Here, the CAL result is lower than its CRB equivalent.

6.3. Total NO_2 results for GOME-2 orbit 2326: CAL vs. CRB

Here, we present similar calculations for the NO_2 DOAS product. Results are not as dramatic as those for ozone. For clear sky AMFs (not shown here), we would expect very little change between CRB and CAL results, particularly in view of the fact that the calculations are based on a fixed profile of NO_2 in the troposphere (this is not the case with ozone). Indeed, differences are always below 0.03% for this case. Figure 13 shows the cloudy-sky AMF differences, plotted against pixel number (top panel), cloud-top albedo (middle panel) and cloud-top height (bottom).

Figure 14 is the resulting plot for VCD differences. In the vast majority of cases, the vertical column amounts differ at most by ±1%, with some minor dependence on cloud fields across the orbit. It is clear that the choice of cloud algorithm is not particular significant for the total NO_2 DOAS algorithm – differences in VCD are much lower than the overall precision of the slant column retrieval. Also, these VCD differences are much lower than uncertainties in AMF values due to lack of knowledge about boundary layer aerosol and surface albedo (these effects alone can generate errors of up to 25% in the product).

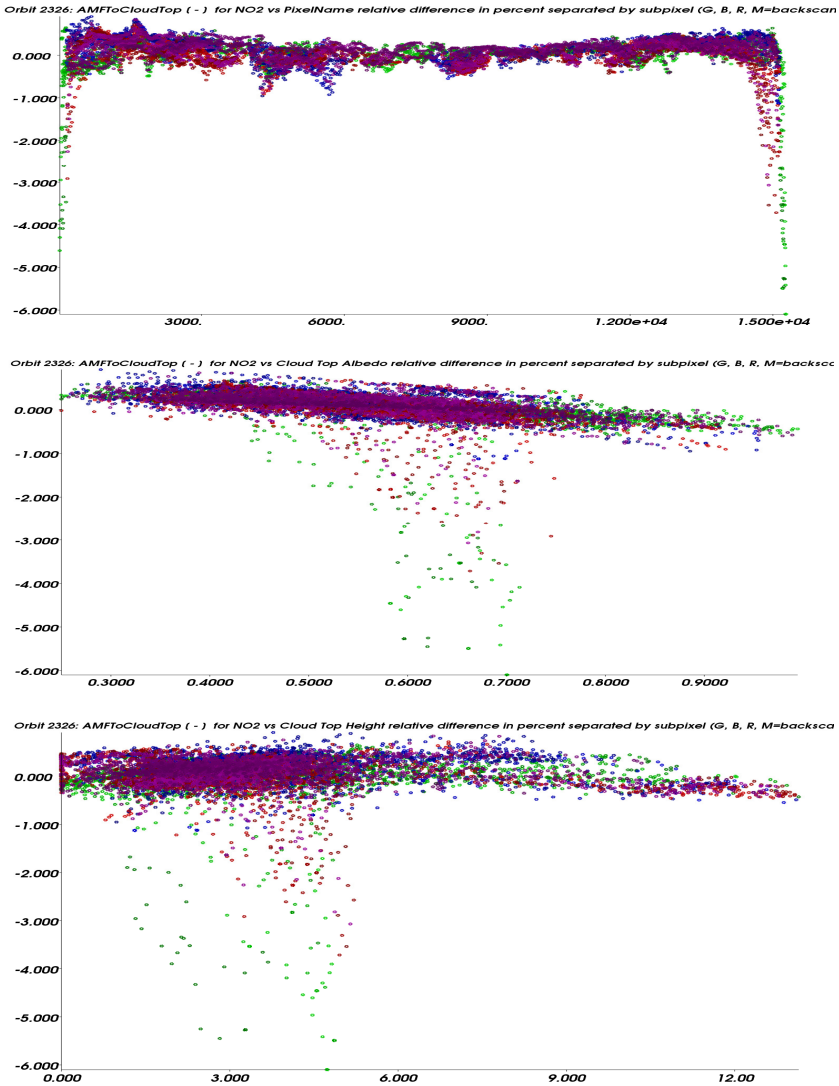

Figure 13. Total column NO_2 cloudy sky AMFs: differences between the CAL and old CRB layering schemes for the GOME-2 orbit # 2326, by pixel number (top panel), cloud-top albedo (middle panel) and cloud-top height (bottom panel).

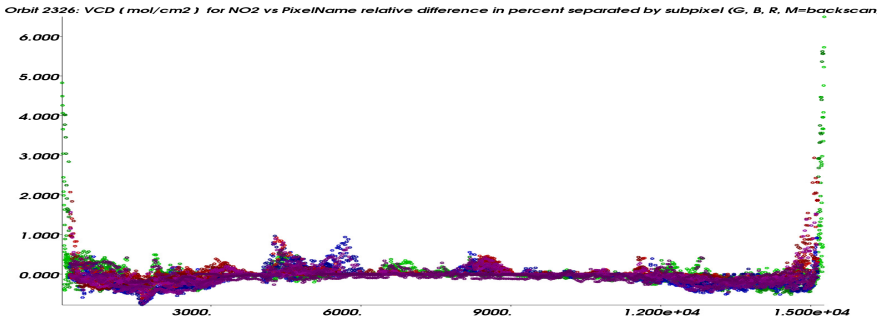

Figure 14. Total column NO_2 VCDs: differences between the CAL and old CRB layering schemes for the GOME-2 orbit # 2326, by pixel number.

6.4. Total O_3 results for 4 GOME-2 orbits (2326,3623,4933,6230)

In this section, we summarize results for four GOME-2 orbits, chosen to traverse different longitudinal zones (Figure 15).

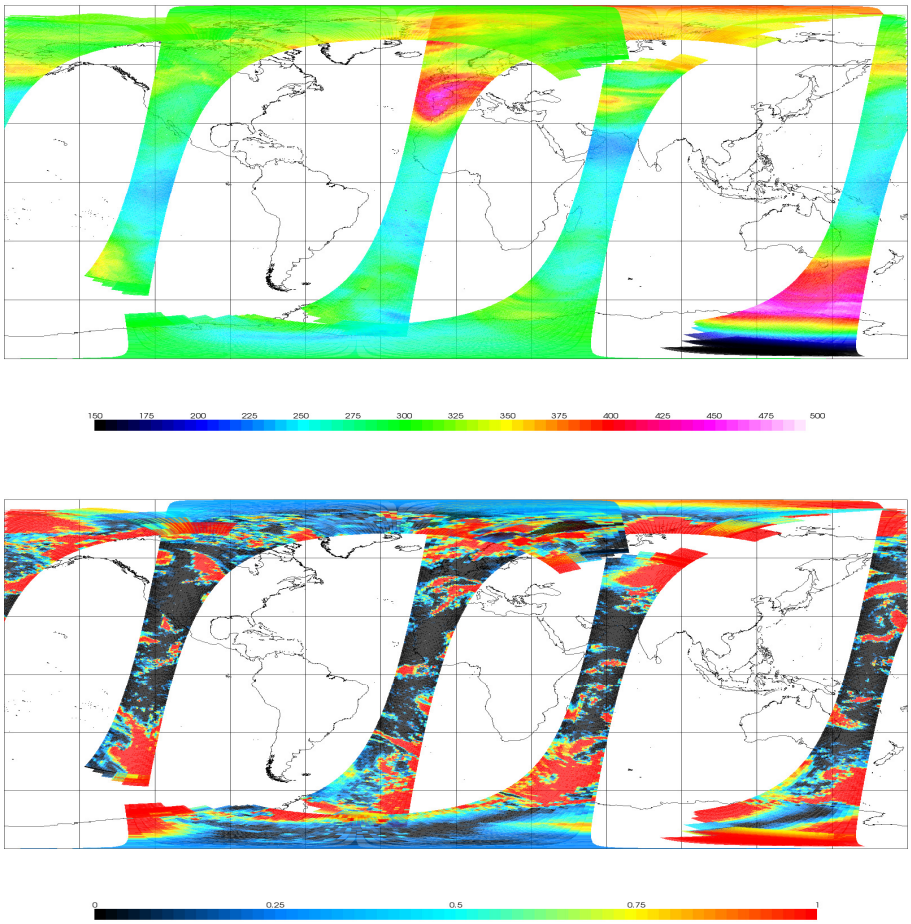

Figure 15. Four GOME-2 orbits used in this study (see text for details). (Top panel) Retrieved total ozone amounts using the CAL treatment are shown; (lower panel) cloud fractional cover.

Results for orbit 2326 (01 April 2007, mid/south Atlantic and Western Europe) have been presented in Section 6.2. The other orbits are 3623 (01 July 2007, North America and Central Pacific), 4933 (01 October 2007, West Pacific and Australia – an ozone hole scenario), and 6230 (01 January 2008, south/west Indian Ocean and Central Asia).

For the CRB results, we have found similar patterns for all four orbits, and for both gases (results not shown here). For ozone, the change in layering scheme has not generated any significant changes to the CRB total ozone product, and for NO_2, relative differences in AMFs and VCDs are still well below the product accuracy level.

It is more interesting to look at O3 CAL products for these 4 orbits. We have found that the results for clear sky AMFs are similar for all four orbits to that presented in Figure 10 (right

panel). [Plots against pixel number will show patterns related to the geographical position of cloud fields in the orbit]. For the cloudy sky AMFs, we have also observed the same biases and dependencies – for cloud-top albedo, results cluster between 1-4 km with a persistent negative bias in the AMF [Figure 11, middle panel], and for cloud-top height there is a clear trend towards lower AMFs with increasing height [Figure 11, middle panel]. These trends are also apparent in the VCDs.

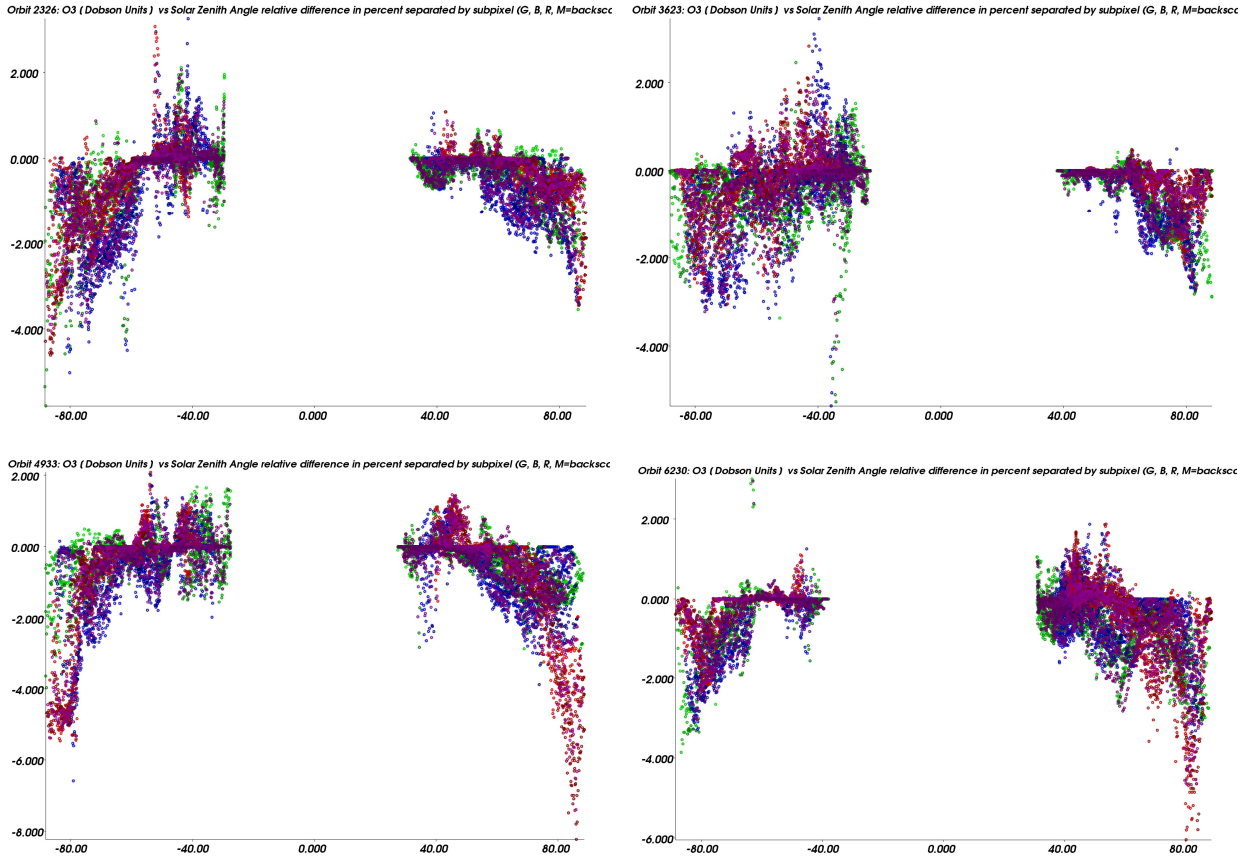

Figure 16. Total column O_3 VCDs: differences between the CAL and old CRB layering schemes for the GOME-2 orbits 2326, 3623, 4933, 6230, by solar zenith angle (negative = northern hemisphere).

Figure 16 shows SZA dependency in total ozone differences, for the four orbits. The orbit progresses from left to right in each of these plots, with the convention to set negative values of SZA for northern hemisphere results. There are a number of difference values close to zero (look at the bars there) – these are groups of clear-sky pixels, for which CAL/CRB differences will be very low. Aside from variations due to individual cloud fields, there is a general negative bias that increases with increasing SZA up to a level of about 3-4%.

For the spring and summer orbits 2326 and 3623 (top panels), results in the southern hemisphere (right-side groupings for positive SZA) show small differences generally below 2%, but having a noticeable but slight SZA dependency. These regions are over the southern oceans (orbits do not reach Antarctica). For these two orbits, most of the northern hemisphere pixels are over land, and there are many results over the arctic. Differences show more variability with cloud cover.

Differences are positive for parts of Africa (2326) and North America (3623). In the spring orbit, there is a marked SZA bias, with differences in northernmost latitudes exceeding 4% at times.

The 4933 orbit (Figure 16, lower left) has strong variation in the southernmost part, with high values just south of Australia and massively reduced values over the Antarctic (ozone hole). Here, the SZA bias is apparent, with differences up to 8% over the ice shelf – interestingly, these differences occur almost exclusively for the red (west) and magenta (backscatter) pixels. Indeed, the pattern of SZA dependency appears to be scan-dependent in this orbit, with the east and center pixels showing a smaller dependency on SZA in general. Caution should be exercised with these comments, since backscatter pixels for example are seldom to be designated cloud-free. It has been known for some time that scan angle biases are present in the GOME-2 total ozone product, though it is not clear from the results pictured here whether the CAL treatment is enhancing or reducing this bias. The scan-position bias is the subject of VS work for 2009.

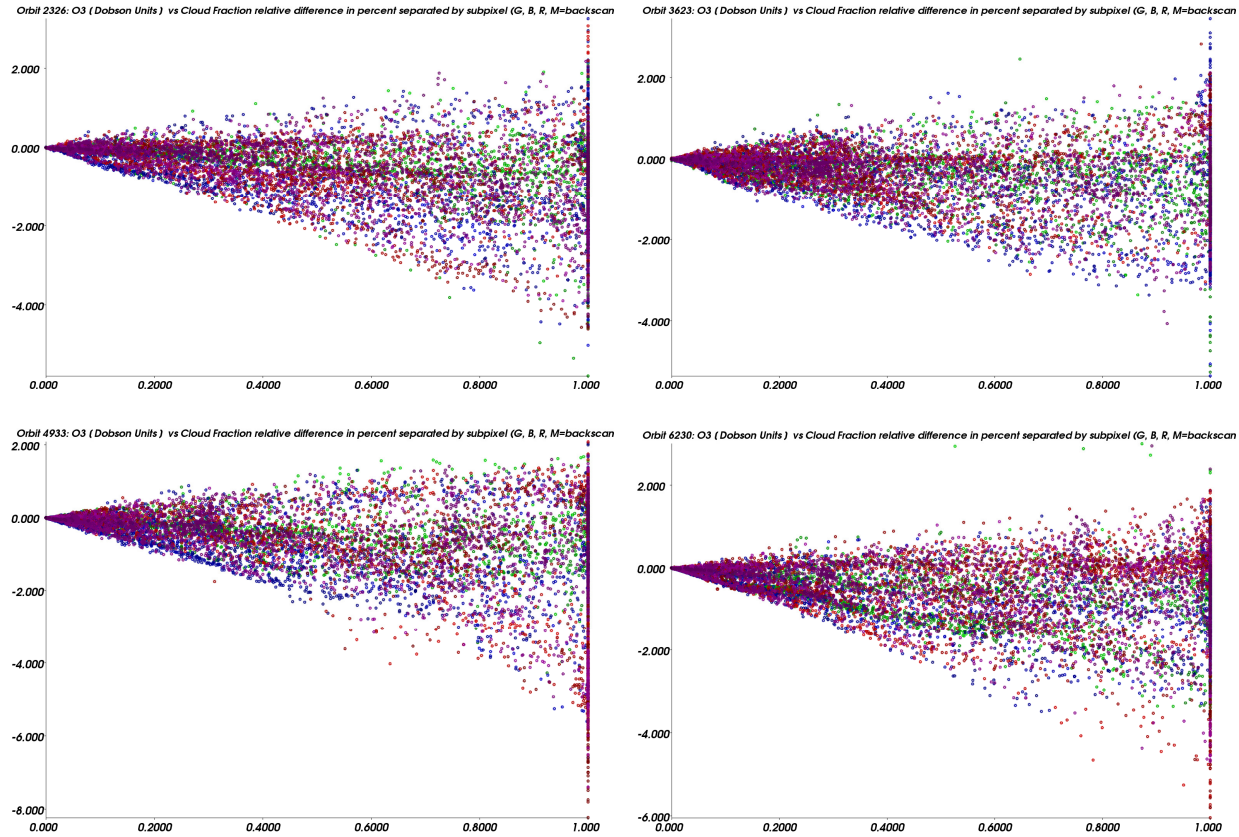

Figure 17. Total column O_3 VCDs: differences between the CAL and old CRB layering schemes for the GOME-2 orbits 2326, 3623, 4933, 6230, by cloud fraction.

Also for this orbit, differences in the Northern Hemisphere for large SZAs are in the range 3-5%, this time for east, west and backscatter pixels, but curiously not center pixels. This may be a feature of enhanced snow cover over the Arctic, where it becomes more difficult to distinguish low cloud from snow. For orbit 6230 (lower right), northern hemisphere results stop well short of the Arctic (see Figure 15, Central Asia), and differences are relatively small. This orbit has a lot of pixels over Antarctica, and there we again see differences up to 8% and the same kind of scan

position dependency seen in orbit 4933.

For orbit 3623 (upper right panel), there are some outliers (green points with large differences around SZA 37 degrees, in the northern hemisphere). The reason for these outliers is not obvious, but they occur for completely cloudy situations with high cloud albedo and high cloud-top height. This is also revealed in Figure 17, which plots the VCD differences for these 4 orbits this time as a function of cloud fraction. From an examination of NOAA Hurricane Reports for the Eastern Pacific in 2008, it turns out that the locations of these outliers coincide with the position s of more than one tropical storm, including Hurricane Boris in the Gulf of California on July 1st.

7. Summary and future work

We have reported on the creation of new clouds-as-layers (CAL) forward modeling scheme for the UPAS total column retrieval algorithms, and the generation of new CAL-based reflectance templates for the ROCINN cloud property algorithm. We have seen that simulated radiances and total ozone Jacobians in the UV Huggins bands are not sensitive to assumed cloud microphysical parameters used in Mie scattering, and that there is little sensitivity to cloud geometrical depth. We have also noted that it is possible to get acceptable radiance accuracy in the UV with a small number of streams in RT model.

For the Interim Report, ROCINN templates were delivered to DLR -In the second phase of the work, the new interfaces and Mie database were successfully integrated into the UPAS system, which was then given a full-scale capability to run whole orbits of GOME-2 using the new CAL and CRB schemes. We used an older method to derive cloud optical thickness from ROCINN-retrieved cloud-top albedo. Initial results for four GOME-2 orbits show substantial differences between CAL cloudy sky AMFs and their CRB equivalents, with corresponding ozone VCD results in general differing by up to 2% (NO_2 up to 1%) in tropics and mid-latitudes. VCD differences are larger at higher latitudes and exhibit an increasing negative-bias solar angle dependency. This may be a good thing, since it is known that the DOAS algorithm in its CRB form tends to overestimate ozone at higher solar zenith angles [*Balis et al.*, 2007].

In 2009, future work will focus on two areas: (1) the implementation of the ROCINN algorithm using the new CAL templates delivered in the present work, and (2) further whole orbit processing and a subsequent first validation of the CAL scheme for DOAS retrievals of GOME total column products. Related work in 2009 will focus on known scan angle dependency in the total ozone product. The work covered by this report will be presented at the 2009 EUMETSAT Meteorological Satellite Conference.

References

Ahmad Z., P.K. Bhartia, and N. Krotkov, Spectral properties of backscattered UV radiation in cloudy atmospheres, *J. Geophys. Res.*, **109**, D01201 (2004).

Balis D., Lambert J-C., van Roozendael M., Spurr R., Loyola D., Livschitz Y., Valks P., Amiridis V., Gerard P., Granville J., Zehner C., Ten years of GOME/ERS-2 total ozone data: the new GOME Data Processor (GDP) Version 4: II. Ground-based validation and comparisons with TOMS V7/V8, . *Geophys. Res.*, vol. **112**, D07307 (2007)

Bodhaine, B., N. Wood, E. Dutton, and J. Slusser, On Rayleigh optical depth calculations, *J. Atmos. Ocean. Tech.*, **16**, 1854-1861, 1999.

Boersma K., H. Eskes, and E. Brinksma, Error analysis for tropospheric NO2 retrieval from space, *J. Geophys. Res.*, **109**, D4, 4311 (2004).

de Rooij, W.A., and C.C.A.H. van der Stap, Expansion of Mie scattering matrices in generalized spherical functions, *Astron. Astrophys*., **131**, 237-248 (1984).

Hahn, C., W. Rossow, and S. Warren, ISCCP cloud properties associated with standard cloud types identified in individual surface observations, *J. Climate*, **14**, 11-28 (2004).

Liu, X., M. Newchurch, R. Loughman, and P.K. Bhartia, Errors resulting from assuming opaque Lambertian clouds in TOMS ozone retrieval, *Journal of Quantitative Spectroscopy and Radiative Transfer*, **85**, 337-365 (2004).

Loyola, D., Automatic Cloud Analysis from Polar-Orbiting Satellites using Neural Network and Data Fusion Techniques, *IEEE IGARS Symposium*, **4**, 2530-2534, Alaska (2004).

Loyola, D., Applications of Neural Network Methods to the Processing of Earth Observation Satellite Data, *Neural Networks*, **19**, 168-177 (2006).

Loyola D., Thomas W., Livschitz Y., Ruppert T., Albert P., Hollmann. R., Cloud properties derived from GOME/ERS-2 backscatter data for trace gas retrieval, *IEEE Transactions on Geoscience and Remote Sensing*, vol. **45**, no. 9, 2747-2758 (2007)

Loyola, D., A semi-transparent Lambertian cloud model for ozone retrieval, DLR presentation, September 2007b.

Loyola, D., W. Thomas, R. Spurr, and B. Mayer, Global Patterns in Daytime Cloud Properties Derived from GOME Backscatter UV-VIS Measurements, *International Journal of Remote Sensing*, in press (2009).

Mayer, B., and A. Kylling, Technical note: The libRadtran software package for radiative transfer calculations - description and examples of use, *Atmos. Chem. Phys.*, **5**, 1855-1877 (2005).

Natraj, V., H. Bösch, R. Spurr, and Y. Yung, Retrieval of XCO2 from Simulated Orbiting Carbon Observatory Measurements using the Fast Linearized R-2OS Radiative Transfer Model. *J. Geophys. Res*., **113**, D11212, doi:10.1029/2007JD009017 (2008).

Rothman, L., et al., The HITRAN 2004 Molecular Spectral Database, *Journal of Quantitative Spectroscopy and Radiative Transfer*, vol. **96**, 139-204 (2005).

Spurr, R., Simultaneous derivation of intensities and weighting functions in a general pseudo-spherical discrete ordinate radiative transfer treatment. *JQSRT*, **75**, 129–175 (2002).

Spurr, R., VLIDORT: A linearized pseudo-spherical vector discrete ordinate radiative transfer code for forward model and retrieval studies in multilayer multiple scattering media, *J. Quant. Spectrosc. Radiat. Transfer*, 102(2), 316-342, doi:10.1016/j/jqsrt.2006.05.005 (2006).

Spurr, R., and D. Loyola, Reflectance Templates for the O_2 A-band OCRA-ROCINN algorithm as applied to GOME-2 retrieval of cloud properties, Final Report, O3M-SAF (2007).

Spurr, R., LIDORT and VLIDORT: Linearized pseudo-spherical scalar and vector discrete ordinate radiative transfer models for use in remote sensing retrieval problems, *Light Scattering Reviews*, VOLUME 3, ed A. Kokhanvsky, Springer (2008).

Tuinder, R. de Winter-Sorkina, and P. Builtjes, Retrieval methods of effective cloud cover from the GOME instrument: An intercomparison, Atmos. Chem. Phys., vol. **4**, no. 1, 255–273 (2004).

Valks P. and D. Loyola, ATBD for GOME-2 Total Column Products of Ozone, Minor Trace Gases, and Cloud Properties, DLR/GOME-2/ATBD/01 (2008)

Van Roozendael, M., D. Loyola, R. Spurr, D. Balis, J-C. Lambert, Y. Livschitz, P. Valks, T. Ruppert, P. Kenter, C. Fayt, and C. Zehner, Ten years of GOME/ERS2 total ozone data: the new GOME Data Processor (GDP) Version 4: I. Algorithm Description, *J. Geophys Res.*, doi: 10.1029/2005JD006375 (2006).